

Gravothermal oscillations in two-component models of star clusters

Philip G. Breen^{1*} and Douglas C. Heggie^{1†}

¹ *School of Mathematics and Maxwell Institute for Mathematical Sciences, University of Edinburgh, Kings Buildings, Edinburgh EH9 3JZ*

1 March 2022

ABSTRACT

In this paper, gravothermal oscillations are investigated in two-component clusters with a range of different stellar mass ratios and total component mass ratios. The critical number of stars at which gravothermal oscillations first appeared is found using a gas code. The nature of the oscillations is investigated and it is shown that the oscillations can be understood by focusing on the behaviour of the heavier component, because of mass segregation. It is argued that, during each oscillation, the re-collapse of the cluster begins at larger radii while the core is still expanding. This re-collapse can halt and reverse a gravothermally driven expansion. This material outside the core contracts because it is losing energy both to the cool expanding core and to the material at larger radii. The core collapse times for each model are also found and discussed. For an appropriately chosen case, direct N -body runs were carried out, in order to check the results obtained from the gas model, including evidence of the gravothermal nature of the oscillations and the temperature inversion that drives the expansion.

Key words: globular clusters: general; methods: numerical; methods: N -body simulations.

1 INTRODUCTION

Gravothermal oscillations are one of the most interesting phenomena which may arise in the post-collapse evolution of a star cluster. The inner regions of a post collapse cluster are approximately isothermal and are subject to a similar instability as the one found in an isothermal sphere in a spherical container, as studied by Antonov (1962) and Lynden-Bell & Wood (1968). Gravothermal oscillations, which are thought to be a manifestation of this instability, were discovered by Bettwieser & Sugimoto (1984) whilst studying the post-collapse evolution of star clusters using a gas model. For a gas model of a one-component cluster it was found that gravothermal oscillations first appear when the number of stars N is greater than 7000 (Goodman 1987). This value of N has also been found with Fokker-Planck calculations (Cohn et al 1989) and by direct N -body simulations (Makino 1996). However, in a multi-component cluster the situation is more complicated. The presence of different mass components introduces different dynamical processes to the system such as mass stratification. Multi-component systems try to achieve kinetic energy equipartition between the

components, which causes the heavier stars to move more slowly and sink towards the centre. This can lead to the Spitzer instability (Spitzer 1987) in which the heavier stars continuously lose energy to the lighter stars without ever being able to reach equipartition. Murphy et al (1990) found that the post-collapse evolution for multi-component models was stable to much higher values of N than in the case of the one-component system and that the value of N at which gravothermal oscillations appeared varied with different mass functions.

In order to gain a deeper understanding of gravothermal oscillations, it is desirable to work with simpler models in which some of the effects which are present in real star clusters are ignored or simplified. For example, real star clusters have a range of stellar masses present, but in the current paper, the stellar masses are limited to two. Gaseous models are often used in this kind of research (Bettwieser & Sugimoto 1984; Goodman 1987; Heggie & Aarseth 1992) because they are computationally efficient. Kim, Lee & Goodman (1998) have already completed research in this area using Fokker-Planck models. However, their research was limited to mostly Spitzer stable models and only a small range of stellar mass ratios. The study in the present paper looks at the more general Spitzer unstable models using various stellar mass and total mass ratios.

* E-mail: p.g.breen@sms.ed.ac.uk

† E-mail: d.c.heggie@ed.ac.uk

There is also evidence of gravothermal oscillations in real star clusters. Giersz & Heggie (2009) modelled the cluster NGC 6397 using Monte Carlo models and found fluctuation in the core radius. Their timescale suggests that they are gravothermal. Subsequently, they confirmed these fluctuations using direct N -body methods with initial conditions generated from the Monte Carlo model (Heggie & Giersz 2009).

Two-component clusters may seem very unrealistic but there is reason to believe that they may be a good approximation to multi-component systems. Kim & Lee (1997) were able to find good approximate matches for half-mass radius r_h , central velocity dispersion v_c , core density ρ_c and core collapse time t_{cc} between two-component models and eleven-component models which were designed to approximate a power law IMF. Also see Kim, Lee & Goodman (1998) for a discussion of the realism of two-component models.

This paper is structured as follows. In Section 2, we describe the models which are used. This is followed by Section 3, in which the results concerning gravothermal oscillations are given. Section 4 is concerned with the results of the core collapse times. In Section 5, the results of N -body simulations are given. Finally Section 6 consists of the conclusions and a discussion.

2 MODELS

2.1 Gas model

2.1.1 Basic equations and Notation

In our model, we ignore primordial binaries and stellar evolution, and assume that the energy generating mechanism is the formation of binary stars in three body encounters and subsequent encounters of binaries with single stars. In a one-component model the rate of energy generation per unit mass is approximately

$$\epsilon = 85 \frac{G^5 m^5 n^2}{\sigma_c^7} \quad (1)$$

(Heggie & Hut 2003), where m is the stellar mass, n is the number density, σ_c is the one dimensional velocity dispersion of the core and G is the gravitational constant. Goodman (1987), whose results on the 1-component model we shall occasionally refer to, used a similar formula, with a coefficient which is, in effect, in the range 140–170 (depending on the value of N).

The equations of the two-component gas model (Heggie & Aarseth 1992) are given below:

$$\frac{\partial M_i}{\partial r} = 4\pi \rho_i r^2 \quad (2)$$

$$\frac{\partial p_i}{\partial r} = -\frac{G(M_1 + M_2)}{r^2} \rho_i \quad (3)$$

$$\frac{\partial \sigma_i}{\partial r} = -\frac{\sigma_i L_i}{12\pi C m_i \rho_i r^2 \ln \Lambda} \quad (4)$$

$$\begin{aligned} \frac{\partial L_i}{\partial r} = & -4\pi r^2 \rho_i \left[\sigma_i^2 \left(\frac{D}{Dt} \right) \ln \left(\frac{\sigma_i^3}{\rho_i} \right) + \delta_{i,2} \epsilon \right. \\ & \left. + 4(2\pi)^{\frac{1}{2}} G^2 \ln \Lambda \left[\frac{\rho_{3-i}}{(\sigma_1^2 + \sigma_2^2)^{\frac{3}{2}}} \right] (m_{3-i} \sigma_{3-i}^2 - m_i \sigma_i^2) \right] \end{aligned} \quad (5)$$

Table 1. Notation (the subscript i corresponds to the i^{th} component, $i = 2$ refers to the more massive component)

r	radius
ρ	mass density
σ	one dimensional velocity dispersion
m	stellar mass
M	total mass (within radius r)
C	Constant (see text)
L	energy flux
N	number of stars
$\ln \Lambda$	coulomb logarithm ($\Lambda = 0.02N$)
$\frac{D}{Dt}$	Lagrangian derivative (at fixed M)
$\frac{\partial}{\partial r}$	radial derivative (at fixed t)

where $i = 1, 2$. This model in turn is ultimately inspired by the one-component model of Lynden-Bell & Eggleton (1980).

The meaning of the symbols can be found in Table 1. The major difference between the above equations and those for the one-component model is the last term of equation 5, which involves the exchange of kinetic energy between the two components. See Spitzer (1987, p.39) for information on this term. As the heavier component dominates in the core of the cluster, it is assumed that all of the energy is that generated from the second component. Hence the Kronecker delta $\delta_{2,i}$ in the last equation. There are two constants in the gas code which can be adjusted: C and the coefficient λ of N in $\Lambda = \lambda N$. The value of $\lambda = 0.02$ was used as it was found to provide a good fit for multi-component models (Giersz & Heggie 1996). The value of C used was 0.104 (Heggie & Ramamani 1989). This value of C results from the comparison of core collapse between gas and Fokker-Planck models of single component systems and it is not clear if it applies accurately to post-collapse two-component models.

2.1.2 The role of N in the gas code

This paper places emphasis on the role of N in evolution, but it is not clear what role N plays in equations (2) – (5). For fixed structure (i.e. $\rho_i(r)$, etc), N appears explicitly in Λ (where its role is rather insignificant), and in the individual masses m_i . These appear in equations (4) and (5). In a system with fixed structure, equation (4) shows

$$L_i \propto m \ln \Lambda \propto \frac{\ln \lambda N}{N},$$

reflecting the fact that the flux L is caused by two-body relaxation, and its time scale is proportional to $\frac{N}{\ln \lambda N}$. In equation (5) N plays a similar role in the last term on the right, which governs the approach to equipartition. It also appears implicitly through ϵ , because of the m dependence in equation (1). For a system of given structure, its contribution to L in equation (5) is proportional to N^{-3} (as we are assuming that $\rho = mn$ is fixed and so ϵ in equation (1) is proportional to m^3). It would seem as though this term is insignificant for large N . In practice, however, the system compensates by increasing the central density so that ϵ

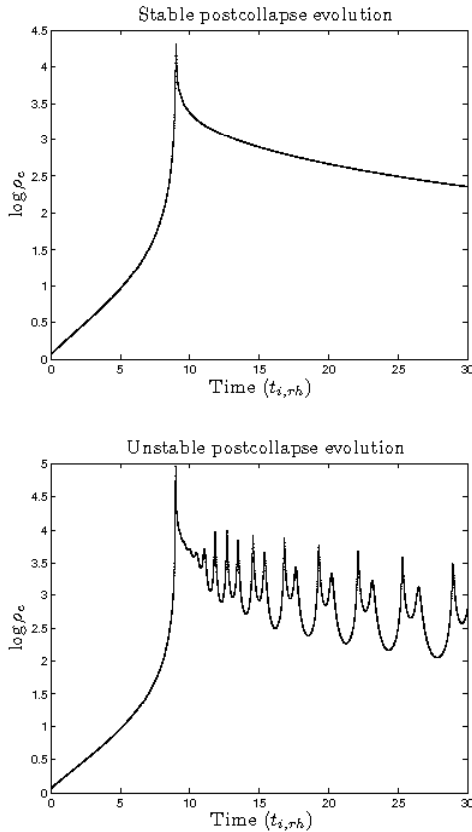


Figure 1. Logarithm of the central density vs time (in units of the initial value of t_{rh}) for a two-component gas model, $\frac{m_2}{m_1} = 2$, $\frac{M_2}{M_1} = 1$, top: $N = 1.5 \times 10^4$ (stable), bottom: 2.5×10^4 (unstable). For initial conditions see Section 3.1

plays a comparable role to the relaxation terms (see Section 3.2.1).

2.2 Direct N -body

Direct N -body simulations were conducted using the NBODY6 code (Aarseth, 2003) enabled for use with Graphical Processing Units (GPU). NBODY6 has a range of features and options such as individual time steps which make it an excellent direct N -body code. NBODY6 is written in FORTRAN and is publicly available for download from www.ast.cam.ac.uk/~sverre/web/pages/nbody.htm.

3 CRITICAL VALUE OF N

If the value of N is not too large, then, after core collapse, the cluster expands at a steady rate (Fig. 1, top). However, at a larger value of N the central density (ρ_c) was found to oscillate (Fig. 1, bottom). Goodman (1987) showed that for one-component models the steady expansion is unstable for large values of N and found that the value at which oscillations first appeared is $N = 7000$. In this present paper, the case of two-component models is investigated.

Table 2. Critical value of N (N_{crit}) in units of 10^4

	1.0	1.7	2.0	2.4	2.8	5.0	8.5	18
$\frac{M_2}{M_1}$	0.5	2.2	2.8	3.5	4.0	7.2	13	30
	0.4	2.3	3.2	3.8	4.6	8.2	15	33
	0.3	2.6	3.6	4.6	5.4	10	18	42
	0.2	3.0	4.4	5.5	7.0	12	22	55
	0.1	3.8	6.0	8.5	10	22	36	100
	2	3	4	5	10	20	50	

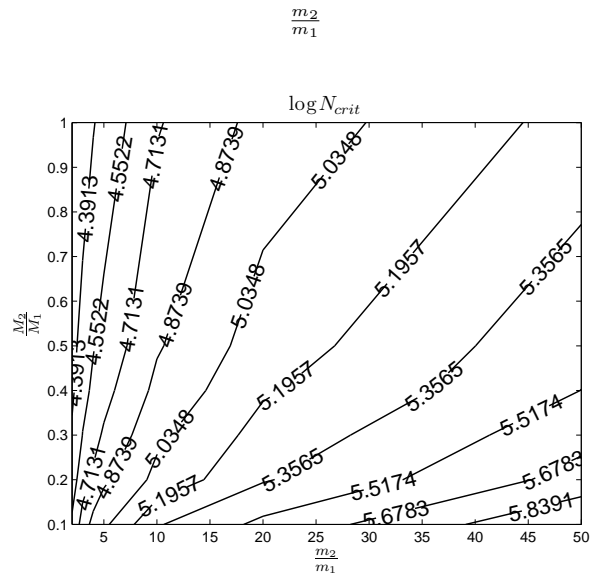


Figure 2. Contours of $\log_{10}(N_{crit})$

3.1 Results of the gas code

In all cases, the initial conditions used were Plummer models (Plummer 1911; Heggie & Hut 2003). The initial velocity dispersions of both components were equal and the initial ratio of density of each component was equal at all locations. The initial conditions were constructed with different stellar mass ratios $\frac{m_2}{m_1} = 2, 3, 4, 5, 10, 20, 50$ and for each of these mass ratios, a model with total mass ratios $\frac{M_2}{M_1} = 0.1, 0.2, 0.3, 0.4, 0.5$ and 1 was constructed. A python script was used to run the gas model code over a range of values of N for each of the pairs of mass ratios. Each run terminated when the time value reached 30 initial relaxation times ($t_{i,rh}$). The value of the central density was checked for an increase in value of 5 percent or more in any interval over the time period between $20t_{i,rh}$ and $30t_{i,rh}$. If an increase was found, the run was deemed to be unstable and the range of N was refined. This process continued until the critical value of N (N_{crit}) at which oscillations first appeared was determined (correct to ten percent). The values of N_{crit} were also visually confirmed from the output of the gas code. The obtained values of N_{crit} in units of 10^4 are given in Table 2. Fig. 2 shows a contour plot of $\log_{10} N_{crit}$.

3.2 Interpretation of the results

In order to attempt to interpret the results in the previous subsection, it is helpful to illustrate the mass density distribution of each component within the cluster and this is done in Fig. 3.

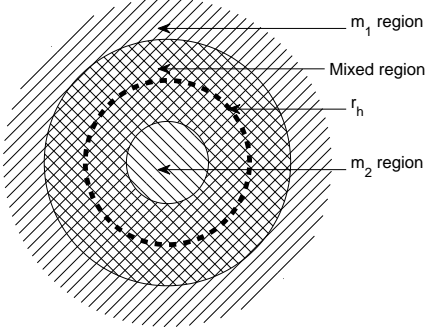


Figure 3. Illustration of mass distribution in star clusters. The dashed line represents r_h , the lines at 135 degrees in the centre represent the area dominated by the heavy component (i.e. $\frac{\rho_2}{\rho_1} \gg 1$), the lines at 45 degrees in the far halo represent the area dominated by the light component (i.e. $\frac{\rho_2}{\rho_1} \ll 1$), the crossed section represents the area where there is a mixture of heavy and light components (i.e. $\frac{\rho_2}{\rho_1} \sim 1$)

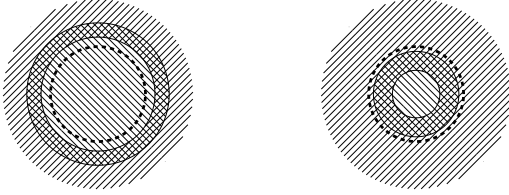


Figure 4. Left: System with $\frac{M_2}{M_1} \gtrsim 1$ and with large enough $\frac{m_2}{m_1}$ to remove most of the light component from within the half mass radius. Right: System with $\frac{M_2}{M_1} < 1$ and $\frac{m_2}{m_1} \gg 1$.

Firstly, let us consider models in which $\frac{m_2}{m_1} \gg 1$. In a region where both components are present at comparable densities, there is a strong tendency towards mass segregation. Therefore, in the region at which $\frac{\rho_2}{\rho_1} \sim 1$, the ratio $\frac{\rho_2}{\rho_1}$ is a rapidly decreasing function of the radius, i.e. the transition region is narrow. Inside this region, m_2 dominates, and m_1 dominates outside. Clearly the radius at which this region is located increases with $\frac{M_2}{M_1}$, and must be near r_h when $\frac{M_2}{M_1} = 1$ (Fig. 4). Finally, for models in which $\frac{m_2}{m_1} \gg 1$, the tendency towards mass segregation decreases, the decrease of $\frac{\rho_2}{\rho_1}$ with r is more gradual, and the transition region is more extensive (Fig. 5). For the same reason the regions dominated by a single component are more restricted than when $\frac{m_2}{m_1} \gg 1$.

3.2.1 Dependence on the number of heavy stars N_2

The values of N_2 at N_{crit} are given in Table 3. The variation in N_2 is considerably less than that of N_{crit} . For large $\frac{m_2}{m_1}$ and fixed $\frac{M_2}{M_1}$, the value of N_2 has approximately the same value, independent of $\frac{m_2}{m_1}$. Now, we give a possible interpretation of this empirical finding that the stability of the system is dominated by the heavy component.

Firstly, let us consider the case of $\frac{M_2}{M_1} \gtrsim 1$ and $\frac{m_2}{m_1} \gg 1$

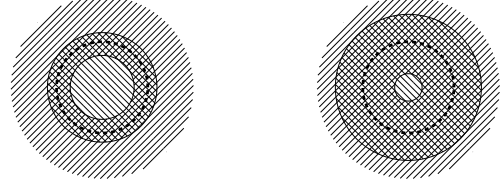


Figure 5. Effect of high and low values of $\frac{m_2}{m_1}$ for a fixed value of $\frac{M_2}{M_1} \sim 1$. Left: high value of $\frac{m_2}{m_1}$. Right: low value of $\frac{m_2}{m_1}$. The mixed region grows with decreasing $\frac{m_2}{m_1}$ and decreases with increasing $\frac{m_2}{m_1}$, because of the enhanced effect of mass segregation.

Table 3. Number of heavy stars (N_2) at N_{crit} in units of 10^4

	1.0	0.57	0.50	0.48	0.47	0.45	0.41	0.35
$\frac{M_2}{M_1}$	0.5	0.44	0.40	0.39	0.36	0.34	0.32	0.30
	0.4	0.38	0.38	0.35	0.34	0.36	0.29	0.26
	0.3	0.34	0.33	0.32	0.31	0.29	0.27	0.25
	0.2	0.27	0.28	0.26	0.27	0.24	0.22	0.22
	0.1	0.18	0.19	0.21	0.20	0.22	0.18	0.20
	2	3	4	5	10	20	50	

$\frac{m_2}{m_1}$

(Fig. 4, left). Within r_h the heavy component dominates and most of the light component is removed to the outer halo. In this case, the light component acts as a container for the heavy component. Here, the stellar mass of the light component is not the most important factor, rather the most important factor is the overall mass of the container. If we were to replace this by an equal mass of stars with stellar mass m_2 , the behaviour of the stars inside r_h would be nearly the same, and so the value of N_2 at the stability boundary would be roughly the same as for a one-component model. Indeed, since part of the container consists of stars of mass m_1 , this could also explain why the values of N_2 are in fact somewhat less than the value of N_{crit} for a one-component system (i.e. 7000, Goodman (1987)) and, in fact, why the critical value of N_2 is decreasing with decreasing $\frac{M_2}{M_1}$. On the other hand, the fact that the critical value of N_2 is less than 7000 may also partly be due to the fact that the energy generation rate, equation (1), is smaller than that used by Goodman. In his paper (Goodman 1987, equation II.26) he shows implicitly that the critical value of N is approximately proportional to the square root of the numerical coefficient in ϵ . At any rate, the arguments we have presented are consistent with the results in the uppermost rows of Table 3.

Secondly, consider the case $\frac{M_2}{M_1} \lesssim 1$ (Fig. 4, right). If the system is Spitzer unstable, the heavy component decouples from the light component and forms its own subsystem. This heavy subsystem can itself become gravothermally unstable and exhibit a temperature inversion in the same way as a one-component model. In this case, however, there is not enough mass in the heavy component to dominate throughout the region within r_h , and so it is not quite as easy to relate this to the one-component case. Rather, we assume that the heavy component behaves like a detached one-component model. However, the basic conclusion is still

the same, the stability of the model is determined by the heavy component. Since the heavy component is again sitting in the potential well of the lighter stars, it is easier for a nearly isothermal region to be set up in the heavier stars than if the entire system consisted of heavy stars, and we again expect N_{crit} to correspond to a lower value of N_2 than in the one-component case.

There is also a noticeable increase in the values of N_2 with decreasing $\frac{m_2}{m_1}$ in the top rows of Table 3. There is currently no clear interpretation of this effect but it may possibly be related to the effect of mass segregation, as the region dominated by the heavy component is larger for larger $\frac{m_2}{m_1}$ (see Fig. 5).

3.2.2 Goodman's stability parameter

Goodman (1993) suggested that the quantity

$$\epsilon \equiv \frac{E_{tot}/t_{rh}}{E_c/t_{rc}} \quad (6)$$

should indicate the stability universally, where $\log_{10} \epsilon \sim -2$ is the stability limit below which the cluster would become unstable. Here E_{tot} is the total energy, E_c is the energy of the core, t_{rc} is the core relaxation time and t_{rh} is the half mass relaxation time. Kim, Lee & Goodman (1998) carried out research using a Fokker-Planck model which seemed to support the condition, although the models they studied were all Spitzer stable.

We have compared the values of ϵ found by Kim, Lee & Goodman (1998) to results obtained from the gas code (Table 4). All the models compared in Table 4, which are the same as those studied by Kim, Lee & Goodman (1998), are stable in the post-collapse expansion as well as being Spitzer stable. An important difference between the Fokker-Planck model used by Kim, Lee & Goodman (1998) and the gas code used in this paper is that Kim, Lee & Goodman (1998) included an energy generation term in both components, whereas the gas code only contains an energy generation term in the heavier component. Therefore, it would be expected, in the case of the gas code, that the core would have to collapse further in order to generate the required amount of energy (from Hénon's principle, see Section 3.3). This could explain the differences in the values of $\frac{r_c}{r_h}$ in Table 4. However, as $\frac{M_2}{M_1}$ increases, the heavier component will dominate in the core and the energy generation of the lighter component will then become negligible. As can be seen in Table 4, there is good agreement between the two results for $\log_{10} \epsilon$ even though there are only small values of $\frac{M_2}{M_1}$. Also, it is possible that Kim, Lee & Goodman (1998) used a different definition of t_{rc} than the one used in this paper (see equation 7). However, as there is such good agreement between the values in Table 4, it is unlikely that Kim, Lee & Goodman (1998) used a significantly different definition. Unlike the other models in the present paper, the models in Table 4 are Spitzer stable. These runs have only been carried out in order to make a comparison of the calculation of ϵ and $\frac{r_c}{r_h}$ using the gas code with the results of Kim, Lee & Goodman (1998). Next we will test the use of epsilon as a stability criterion for Spitzer unstable cases.

We tested the stability criterion based on equation (6)

Table 4. Comparison of values of ϵ and $\frac{r_c}{r_h}$

$\frac{m_2}{m_1}$	$\frac{M_2}{M_1}$	N	Kim et al $\log \epsilon$	Gas model $\log \epsilon$
2	0.02	3×10^4	-1.620	-1.553
3	0.03	3×10^4	-1.224	-1.167
3	0.03	10^5	-1.597	-1.544

$\frac{m_2}{m_1}$	$\frac{M_2}{M_1}$	N	Kim et al $\frac{r_c}{r_h}$	Gas model $\frac{r_c}{r_h}$
2	0.02	3×10^4	7.03×10^{-3}	4.86×10^{-3}
3	0.03	3×10^4	1.31×10^{-2}	0.91×10^{-2}
3	0.03	10^5	5.38×10^{-3}	3.93×10^{-3}

Table 5. Value of $\log \epsilon$ for largest stable run

$\frac{M_2}{M_1}$	1.0	-1.65	-1.78	-2.15	-2.75
0.5	-1.68	-1.90	-2.15	-2.75	
0.2	-1.65	-1.84	-1.95	-2.48	
	2	5	10	50	
$\frac{m_2}{m_1}$					

for the subset of models given in Table 5. For each fixed $\frac{M_2}{M_1}$ and $\frac{m_2}{m_1}$, the values of ϵ were found to decrease with increased N up until the post-collapse evolution became unstable. The values of $\log_{10} \epsilon$ given in Table 5 are the values for the run with the highest stable N . As can be seen from Table 5 the value of $\log_{10} \epsilon$ is indeed in the region of -2 . However, the limiting value of stable ϵ varies with $\frac{m_2}{m_1}$ and to a much lesser extent with $\frac{M_2}{M_1}$.

Now we shall try to improve upon the definition of ϵ . In equation (6), t_{rc} and t_{rh} are defined by

$$t_{rc} = \frac{0.34\sigma_{c,2}^3}{G^2 m_2 \rho_{c,2} \ln \Lambda} \quad (7)$$

and

$$t_{rh} = \frac{0.138 N^{\frac{1}{2}} r_h^{\frac{3}{2}}}{(G\bar{m})^{\frac{1}{2}} \ln \Lambda}. \quad (8)$$

Note that t_{rc} was defined using the properties of the heavy component in the core rather than the averages of both components, as the heavy component dominates in the core. However t_{rh} (equation (8)) depends on N and \bar{m} , which can vary dramatically with $\frac{m_2}{m_1}$ and $\frac{M_2}{M_1}$ for fixed N_2 whereas, as argued in Section 3.2, the important criterion is the number of heavy stars. We suggest that a modified version of the Goodman stability parameter could be constructed using a relaxation time based on the heavy component in place of t_{rh} . For example, if $\frac{M_2}{M_2} \gtrsim 1$ and we assume that the heavier component dominates within r_h , then the properties of the system within r_h would be roughly similar to that of a one-component system with the same total mass. We can attempt to treat the system as if it consisted entirely of the heavy component with an effective number of stars $N_{ef} = \frac{M}{m_2}$. The half mass relaxation time of this one-component system would be

Table 6. $\log \epsilon$ and $\log \epsilon_2$ for the case $\frac{M_2}{M_1} = 1$

$\log \epsilon$	-1.65	-1.78	-2.15	-2.75
$\log \epsilon_2$	-1.51	-1.39	-1.53	-1.56
$\frac{m_2}{m_1}$	2	5	10	50

$$t_{rh,ef} = \frac{0.138 N_{ef}^{\frac{1}{2}} r_h^{\frac{3}{2}}}{(Gm_2)^{\frac{1}{2}} \ln \lambda N_{ef}} = \left(\frac{1 + \frac{M_2}{M_1}}{\frac{M_2}{M_1} + \frac{m_2}{m_1}} \right) \left(\frac{\ln \lambda N}{\ln \lambda N_{ef}} \right) t_{rh}.$$

We can define a modified stability condition by replacing t_{rh} with $t_{rh,ef}$ in the definition of ϵ which would then give the following condition

$$\epsilon_2 \equiv \frac{E_{tot}/t_{rh,ef}}{E_c/t_{rc}}.$$

The values of $\log_{10} \epsilon$ and $\log_{10} \epsilon_2$ are compared in Table 6 for the case $\frac{M_2}{M_1} = 1$. The values of $\log_{10} \epsilon_2$ are in much better agreement with each other than those of $\log_{10} \epsilon$ and suggest that a better stability condition is $\log_{10} \epsilon_2 \approx -1.5$ rather than $\log_{10} \epsilon \approx -2$. For the cases with $\frac{M_2}{M_1} \lesssim 1$ it is unclear how to define an appropriate relaxation time, and so we will not consider the modified stability condition for those cases.

To summarise, the values of ϵ (and especially ϵ_2) seem to give an indication of stability for the two-component models but the values of ϵ were found to change with different conditions (e.g. $\frac{m_2}{m_1}$). The critical value of ϵ_2 is much less variable. The critical value of $\log_{10} \epsilon$ or $\log_{10} \epsilon_2$ is still to be tested for multi-component models, and this would be an interesting topic for further research.

3.3 Weak oscillations

Hénon (1975) suggested that the energy generation rate of the core is determined by the requirement that it meets the energy demands of the rest of the cluster. This demand is normally thought of in terms of the energy flux at the half mass radius. We shall refer to this as Hénon's principle. This principle, together with the notion of gravothermal instability, is the basis of the usual qualitative picture of gravothermal oscillations (Bettwieser & Sugimoto 1984), which we now recap.

In a situation with very large N , the core has to collapse to a small size in order to meet the required energy generation. The steady state is gravothermally unstable, as there would be a large density contrast in a nearly isothermal region. If the core is generating more energy than can be conducted away, this would cause the core to expand, cool and reduce its rate of energy generation. If there is sufficient expansion, then the core would be cooler than its surroundings. This would result in the core starting to absorb heat. Since the core has a negative specific heat capacity, this would cause the core to expand further and become even cooler than before (Bettwieser & Sugimoto 1984). Ultimately, however, the core must collapse again to meet the energy requirements of the rest of the cluster. Here, we adapt this explanation of gravothermal oscillations to the case of two-component clusters.

In one-component gas models, as N increases the instability first appears in the form of periodic oscillations¹ (Heggie & Ramamani 1989). In order to study the instability for the case of weak or low amplitude oscillations in our two-component model, a model was chosen which demonstrated periodic oscillation with parameters $\frac{m_2}{m_1} = 2$, $\frac{M_2}{M_1} = 1$ and $N = 2.0 \times 10^4$ (the value of N_{crit} for $\frac{m_2}{m_1} = 2$, $\frac{M_2}{M_1} = 1$ is 1.7×10^3 from Table 2). Fig. 6 plots $\ln \rho$ at various fixed values of $\log r$ for this model. The total energy flux L is shown in Fig. 7 over the particular expansion phase from $24.54t_{i,rh}$ to $25.18t_{i,rh}$ and the contraction phase from $25.18t_{i,rh}$ to $26.52t_{i,rh}$. Fig. 8 shows the profiles of $\log \rho$ and $\log \sigma^2$ over the expansion phase from $24.54t_{i,rh}$ to $25.18t_{i,rh}$.

During the expansion of the core, the flux in the inner region (between r_c and r_h) drops and eventually becomes negative (Fig. 7, top) in a small range of the radius. At this point there is an inwards flux of energy to the core. Since the core has a negative heat capacity, it would be expected that this would enhance the negative flux and therefore the expansion. However, the expansion stops at this point. This is similar to behaviour observed by McMillan & Engle (1996). Now we explain why this happens. Hénon (1975) argues that the flux at r_h must be maintained, and we note that there is always a positive flux at the half-mass radius r_h . Since the flux from the core becomes negative at some radius between r_c and r_h , there must be a positive flux gradient in some region between the core and half mass radius. This can be seen in Fig. 7 (top) towards the end of the expansion and it continues into the early part of the contraction phase (Fig. 7, bottom).

The flux gradient can be related to density via equation (5). As the heavier component dominates in the inner regions (see Fig. 8), the main contribution to the flux is from the heavier component (i.e. $L \sim L_2$). Outside the core the energy generation will be negligible. Finally, the temporal change in $\ln \rho$ is greater than that in $\ln \sigma^3$. Taking all of this into account and rearranging equation (5) will result in the following:

$$\frac{1}{r^2 \rho_2 \sigma_2^2} \frac{\partial L}{\partial r} \simeq \left(\frac{D}{Dt} \right) \ln \left(\frac{\rho_2}{\sigma_2^3} \right) \simeq \left(\frac{D}{Dt} \right) \ln \left(\rho_2 \right). \quad (9)$$

Since all of the coefficients of the flux gradient are positive the sign of flux gradient must be the same as that of the Lagrangian derivative of the density. Thus a positive radial flux gradient in space implies that the density is increasing with time. This can be seen in Fig. 6, where the dashed lines mark the moment when the contraction becomes an expansion, and the solid lines mark the time when contraction resumes. It is clear that the contraction begins at large radii ($\log r \gtrsim -1.6$) while the core is expanding, and that this region of contraction propagates inwards at later times. This can be related to the position of the positive gradient in Fig. 7 via the above equation (as long as the density is low enough that energy generation is negligible). Therefore, the collapse of the parts of the cluster between the core and r_h starts while the core is expanding, and brings the expansion to a halt. Note that Fig. 6 is density plotted at fixed radius whereas time-derivatives in equation 9 are at fixed mass.

¹ Strictly, only periodic if one scales out the steady expansion

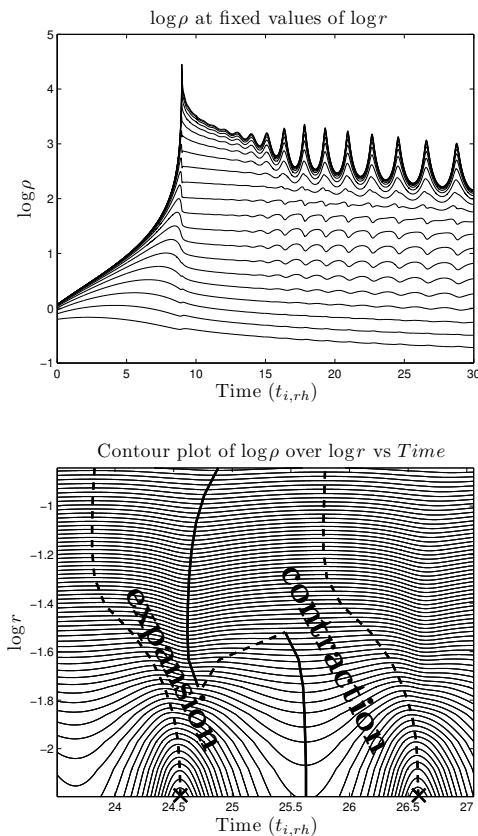


Figure 6. Values of $\log \rho$ at fixed values of $\log r$ in the range -2.7621 to -0.5038 in equal steps of size 0.1129 , for two-component models with $\frac{m_2}{m_1} = 2$, $\frac{M_2}{M_1} = 1$ and $N = 2.0 \times 10^4$. Bottom: contour plot of $\log \rho$; the dashed lines represent the point of highest density reached locally over the time interval $23.5t_{i,rh}$ to $26.7t_{i,rh}$ and solid lines are the regions of lowest density reached between the dashed lines. \times marks the points of core bounce, where the core stops contracting and starts expanding

Nevertheless in Fig. 6 we can also see that there are intermediate radii in which the density evolves in the opposite way from the core.

Although we have constructed the details of this description in the context of two-component models, nothing we have said depends entirely on this, and it seems likely that similar ideas will apply to one-component and multi-component models.

4 CORE COLLAPSE TIME

While it may seem that the study of core collapse times is inappropriate in the context of gravothermal oscillations, it can be argued that the collapse phase of a gravothermal oscillation is not essentially different from the phenomenon of core collapse. Furthermore, another reason for its inclusion is that the evolution of isolated two-component models is an interesting research topic in its own right, and with the aim of constructing a comprehensive approximate theory of these models, studying the core collapse time is an appropriate first step.

The core collapse time t_{cc} for a one-component cluster

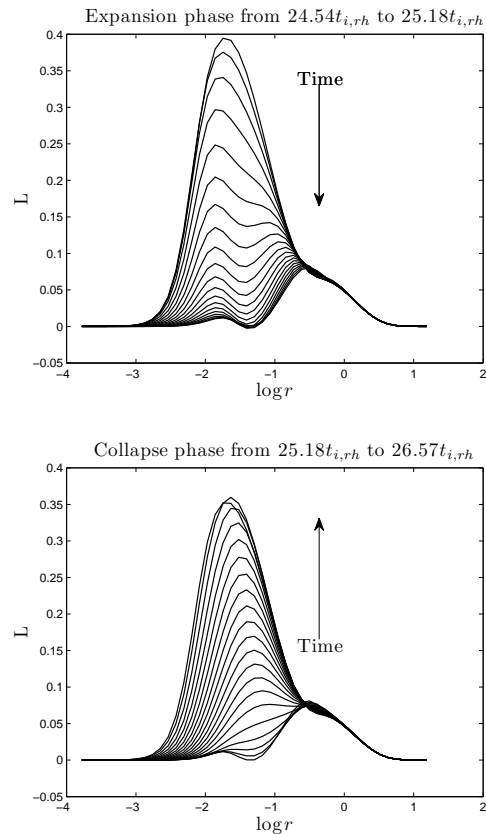


Figure 7. Total energy flux in a two-component model with $\frac{m_2}{m_1} = 2$, $\frac{M_2}{M_1} = 1$ and $N = 2.0 \times 10^4$. The expansion phase from $24.54t_{i,rh}$ to $25.18t_{i,rh}$ is on the top and the contraction phase from $25.18t_{i,rh}$ to $26.57t_{i,rh}$ is on the bottom

with Plummer model initial conditions has been found to be approximately $15.5t_{i,rh}$ (Binney & Tremaine 2008; Heggie & Hut 2003) using various methods. Takahashi (1995) found a longer t_{cc} of $17.6t_{i,rh}$ with a one-component anisotropic Fokker-Planck code. However, the presence of a range of stellar masses can have a dramatic effect on the collapse time because of the process of mass segregation. The effect of mass segregation in multi-component models has been studied using Fokker-Planck calculations (Murphy et al 1990; Chernoff & Weinberg 1990) and Monte Carlo methods (Gürkan et al 2004). The effect of mass segregation in two-component models has already been studied extensively using direct N -body methods (Khalisi et al 2007).

For the gas model runs discussed in Section 3, Table 7 gives the values of the collapse time in units of the initial half mass relaxation time. Fig. 9 shows a contour plot of $\log t_{cc}$. The fastest collapse times occur with models of low $\frac{M_2}{M_1}$ and high $\frac{m_2}{m_1}$.

For two-component systems, the timescale of mass segregation varies as $(\frac{m_2}{m_1})^{-1}$ (Fregeau et al 2002, and references therein). As mass segregation enhances the central density, it is expected that the mass segregation timescale is comparable with the timescale of core collapse. Fig. 10 compares the variation of the timescale of core collapse with the expected timescale of mass segregation. For the case of $\frac{M_2}{M_1} = 1.0$ (top line in Fig. 10) the collapse time indeed appears to vary as $(\frac{m_2}{m_1})^{-1}$. However, for lower values of $\frac{M_2}{M_1}$, the core collapse

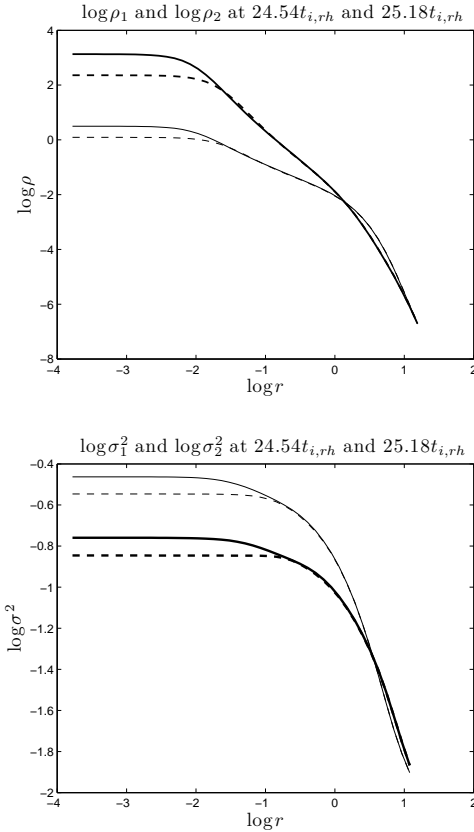


Figure 8. Profiles of $\log_{10}(\rho)$ (top) and $\log_{10}(\sigma^2)$ (bottom) for each component at maximum (dashed line) and minimum (solid line) expansion over times shown in Fig. 7. The heavy (light) curves refer to the more (less) massive component

Table 7. Collapse time t_{cc} in units of the initial relaxation time

	1.0	8.95	7.80	4.78	3.87	2.0	1.1	0.5
$\frac{M_2}{M_1}$	0.5	7.80	4.78	3.45	2.75	1.38	0.72	0.35
	0.4	7.58	4.43	2.89	2.49	1.23	0.66	0.31
	0.3	7.44	4.17	2.88	2.24	1.1	0.55	0.20
	0.2	7.42	3.89	2.65	1.97	0.91	0.47	0.16
	0.1	8.1	3.95	2.4	1.7	0.75	0.38	0.13
	2	3	4	5	10	20	50	
	$\frac{m_2}{m_1}$							

time decreases more quickly than for $(\frac{m_2}{m_1})^{-1}$. Khalisi et al (2007) also found a steeper decrease of the core collapse time in their study, for the case $\frac{M_2}{M_{i,tot}} = 0.1$, where $M_{i,tot}$ is the initial total cluster mass.

We can attempt to improve on these ideas at least qualitatively by considering in more detail a Spitzer unstable model. In that case, we can separate the pre-collapse evolution of the cluster into an initial mass segregation-dominated stage and a later gravothermal collapse-dominated stage, in which the centrally concentrated heavy component behaves almost as a one-component system thermally detached from the lighter component. We propose that this separation can be located via the minimum of the rate of change of central density ratio (i.e $\min \{ \frac{d}{dt} (\frac{\rho_2}{\rho_1}) \}$). The reasoning behind this is as follows: as time passes, the increase in the den-

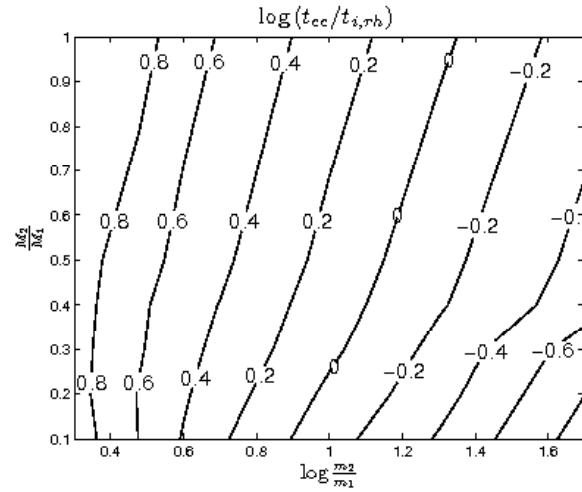


Figure 9. Contours of $\log(\frac{t_{cc}}{t_{i,rh}})$ as a function of M_2/M_1 and m_2/m_1 .

sity ratio caused by mass segregation starts to slow due to a combination of decreasing relative density and increasing temperature of the lighter component in the central regions. We assume that it is at this point that the gravothermal collapse of the heavier component becomes the dominant behaviour of the system. The gravothermal collapse in the heavy component increases the temperature of the heavy component, and because the light component absorbs energy from the heavy component, the collapse of the heavy component causes a deceleration in the collapse of the light component. This in turn enhances the rate of increase in the density ratio.

Fig. 11 shows the density ratio ρ_2/ρ_1 vs time for $N = 10000$ and $\frac{M_2}{M_1} = 1, 0.1$. For the case of $\frac{m_2}{m_1} = 2$ (the lowest curve) there is a clear distinction between the part before the point of inflection at about $\frac{t}{t_{i,rh}} = 5$ (i.e the initial mass segregation phase) and the part after the point of inflection (i.e the gravothermal collapse phase). As $\frac{m_2}{m_1}$ increases the initial phase dominated by mass segregation becomes more substantial and eventually the initial mass segregation phase brings the system all the way to core bounce. However, as N increases, binary energy generation becomes less efficient relative to the energy demands of the cluster (Goodman 1987). Therefore, the core needs to reach a higher density at core bounce for larger N . As the initial phase of mass segregation is self limiting for the reason given above, mass segregation cannot increase the central density beyond a certain point. Therefore, it would be expected that the gravothermal collapse dominated phase must eventually return with increasing N for any given $\frac{M_2}{M_1}$ and $\frac{m_2}{m_1}$.

5 DIRECT N -BODY

Bettwieser & Sugimoto (1985) compared N -body systems to gaseous models using a direct $N = 1000$ model. Even though the value of N is small by today's standards there was still fair agreement during the pre-collapse phase. There were large statistical fluctuations in the post-collapse phase and this was most likely due to the small particle number.

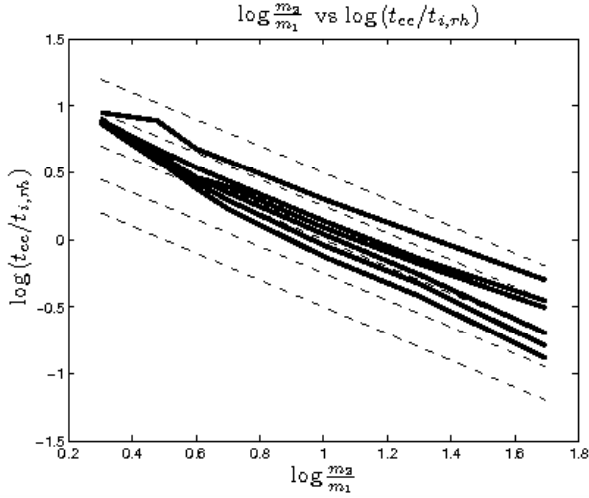


Figure 10. Solid lines are $\log(\frac{t_{cc}}{t_{i,rh}})$ vs $\log \frac{m_2}{m_1}$; from top to bottom $\frac{M_2}{M_1} = 1.0, 0.5, 0.4, 0.3, 0.2$ and 0.1 . Dashed lines are $\log(k \frac{m_1}{m_2})$ vs $\log \frac{m_2}{m_1}$ for various values of k .

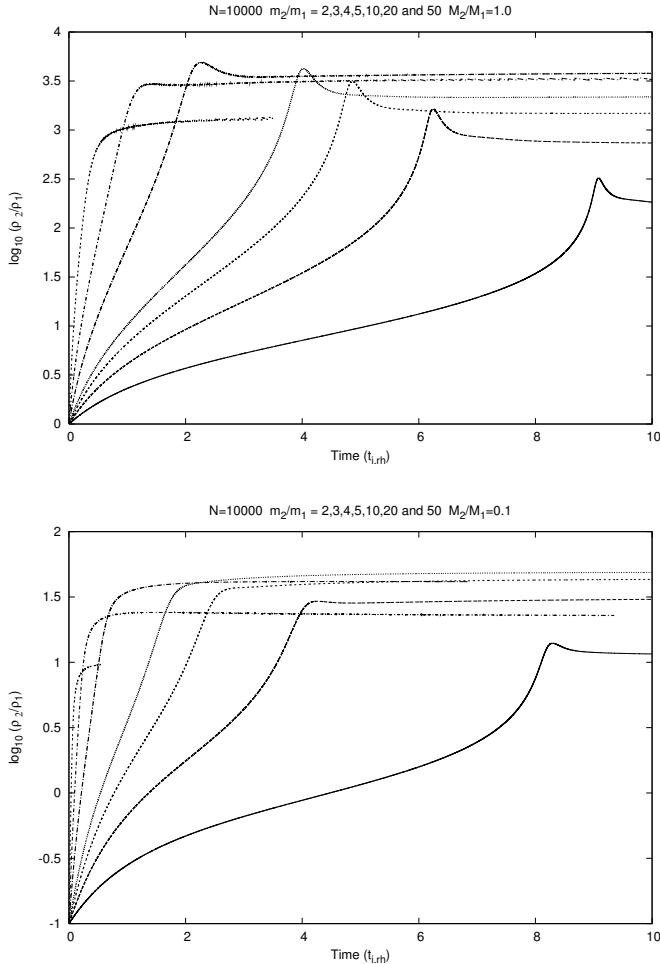


Figure 11. $\log_{10}(\frac{\rho_2}{\rho_1})$ vs time (in units of $t_{i,rh}$) for the case of $\frac{M_2}{M_1} = 1$ (top) and $\frac{M_2}{M_1} = 0.1$ (bottom). Curves from bottom to top are $\frac{m_2}{m_1} = 2, 3, 4, 5, 10, 20$ and 50 .

Table 8. Collapse time t_{cc}

N	8k	16k	32k	64k
N -body units	1160	1990	3480	6380
$t_{i,rh}$	7.76	7.56	7.41	7.51

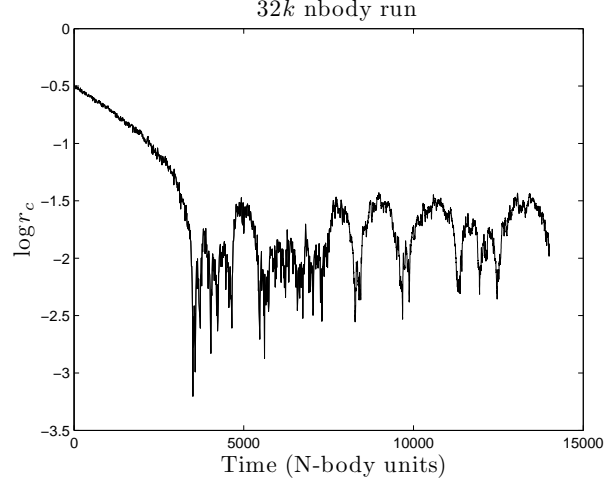


Figure 12. $\log_{10} r_c$ vs time, where r_c is defined as in NBODY6, $\frac{m_2}{m_1} = 2$, $\frac{M_2}{M_1} = 1$ and $N = 32k$.

However, it is still important to confirm a sample of the results of the gas model by using a direct N -body code.

The case of $\frac{m_2}{m_1} = 2$ $\frac{M_2}{M_1} = 1$ was chosen because it had the smallest value of N_{crit} . The values of N used for these runs were 8k, 16k, 32k and 64k. The collapse times of the runs in N -body units (see Heggie & Mathieu 1986) and units of $t_{i,rh}$ are given in Table 8. The average collapse time measured in units of $t_{i,rh}$ is about 7.5 which is lower than the predicted value of 8.95 in Table 7. The difference in collapse time could be because of the approximate treatment of two-body relaxation in the gas model, the neglect of escape, or parameter choices in the gas code (Section 2.1).

For the case of the runs with N equal to 8k and 16k no behaviour was found which could be described as gravothermal oscillation. This is in agreement with the gas code, which gave $N_{crit} = 17000$. However, the 32k case does show a cycle of expansion and contraction of the core over the time interval 4500 to 5500 N -body units (see Fig. 12). In order to check that the expansion was not driven by sustained binary energy generation, we consider the evolution of the relative binding energy $\frac{E_b}{E}$, where E_b is the total binding energy of the binaries and E is the absolute value of the total energy of the cluster, over this time period. This is plotted in Fig. 13 along with the core radius. There are small changes in the binding energy of binaries over this period, decreases as well as increases, but this cannot fully account for the expansion phase that is observed, as there are other periods with similar binary activity in which no sustained expansion occurs. Also, the time scale of the expansion is much longer than the relaxation time in the core (~ 0.5 in N -body time units). Therefore, we assume that the expansion must be driven by

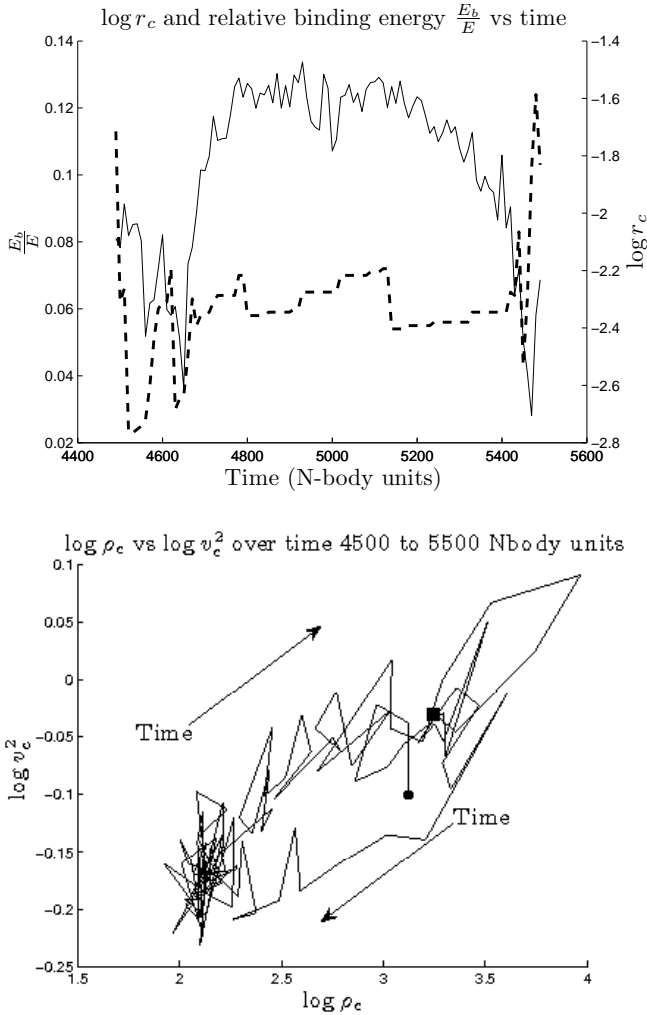


Figure 13. 32k N -body results. Top: relative binding energy $\frac{E_b}{E}$ compared to $\log r_c$ over time 4500 to 5500 N -body units. Bottom: $\log r_c$ vs $\log v_c^2$ over the same time period, where, \bullet and \blacksquare represent the starting and finishing points.

phenomena outside the core, and gravothermal behaviour is a plausible explanation.

Several other pieces of evidence point to this conclusion. Fig. 14 shows the density in Lagrangian shells of the heavier component. As discussed in Section 3.3 (e.g. Fig. 6, top) the region further away from the core is seen to contract while the core expands. Also, in the cycle of $\ln \rho_c$ vs the core velocity dispersion $\log v_c^2$, the temperature is lower during the expansion where heat is absorbed and higher during the collapse where heat is released (Fig. 13, bottom). This is similar to the cycles found by Makino (1996) for one-component models and is another sign of gravothermal behaviour. The results from the 32k gas run are shown in Fig. 15 for comparison.

The 64k run shown in Figs. 16 and 17 has large amplitude oscillations. There is a part of the expansion which is shown in Fig. 17 between 7353 and 7390 in which the relative binding energy of binaries is nearly constant. Therefore binary activity cannot be what is driving the expansion. Fig. 17 (bottom) shows the evolution of the profile of $\log v^2$ over part of the expansion. A negative temperature gradient is

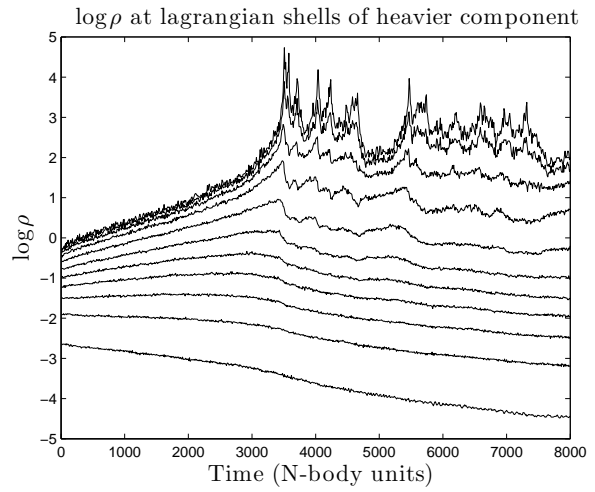


Figure 14. 32k N -body results. $\log \rho$ in Lagrangian shells of 1, 2, 5, 10, 20, 30, 40, 50, 62.5, 75 and 90 percent mass in the heavier component. It can be seen that the collapse at 5400 starts further out (while the core is still expanding) and propagates towards the core.

visible towards the end of this expansion and this is what is driving the expansion. From the results of the 32k and 64k runs it seems that the value of $N_{crit} = 17000$ obtained by the gas code is a reasonable indicator of stability for the N -body case in the sense that none of the signs of gravothermal behaviour were found for $N \lesssim 16k$.

6 CONCLUSIONS AND DISCUSSION

The main focus of this paper has been on the gravothermal oscillations of two-component systems. The critical value of N for the onset of instability has been found for a range of stellar mass ratios and total mass ratios using a gas model. The case of $\frac{M_2}{M_1} = 1$ and $\frac{m_2}{m_1} = 2$ was further investigated using the direct N -body code NBODY6. The value of N_{crit} obtained from the gas code seems to be a good indicator for stability in N -body runs for this case. Based on this, it is a reasonable assumption that the other N_{crit} values would give an indication of the stability for direct N -body systems. The values of N_{crit} for the two-component model were found to be much higher than for the one-component case and were found to vary with $\frac{m_2}{m_1}$ and $\frac{M_2}{M_1}$. However, the value of N_2 at the stability limit was found to vary much less than N itself. This seems to suggest that instability depends on the properties of the heavy component (see 3.2). A possible explanation of this is given in Section 3.2.

The physical manifestation of the oscillations was investigated for the case of small-amplitude periodic oscillations in the gas model. It has been pointed out that the collapse of the region between r_c and r_h is an important mechanism which can halt the expansion phase of a gravothermal oscillation. This mechanism should also be present in one-component models and it would be an interesting topic for future work to see how this mechanism would behave with different stellar mass functions.

Kim, Lee & Goodman (1998) argued that two-component clusters may be realistic approximations of

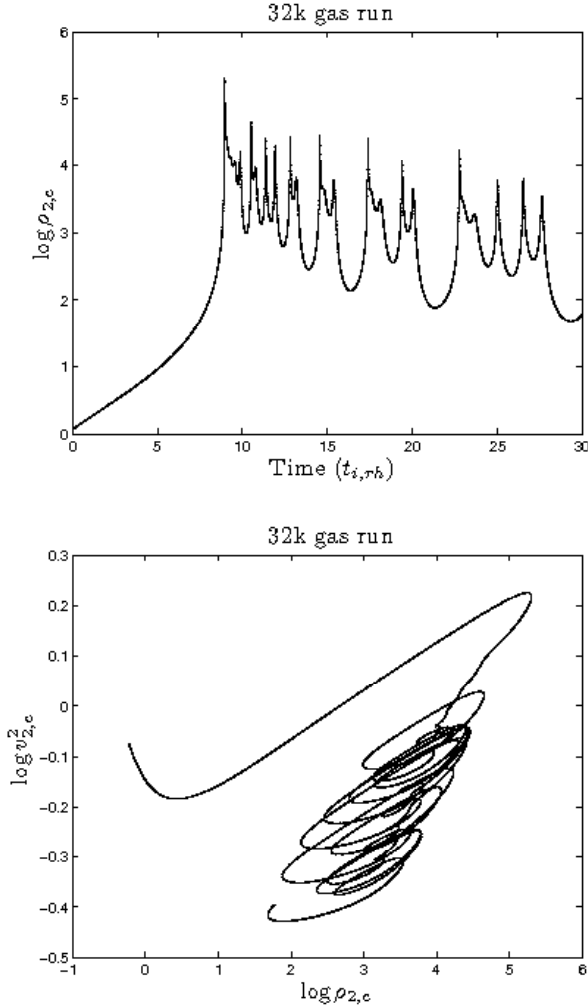


Figure 15. Evolution of the central properties of the heavy component in a 32k gas model. Top: $\log \rho_{2,c}$ vs time (units $t_{i,rh}$), bottom: $\log \rho_{2,c}$ vs $\log v_{2,c}^2$. All cycles are clockwise. The initial drop in $\log v_{2,c}^2$ results from the two components trying to achieve thermal equilibrium

multi-component clusters, where the two components are neutron stars and main sequence stars and the effect of white dwarfs (heavier than the turnoff mass) was assumed to be negligible. They also only studied cases that were Spitzer stable, which means that the components were able to achieve equipartition of kinetic energy. For the two-component case, it is only possible for it to be Spitzer stable if there is only a small amount of the heavier component present. As there is a significant range of stellar masses in a real star cluster, it is likely that some form of the Spitzer instability will be present.

To apply our ideas to a multi-component system, it may be possible to group the heavier components together if they are able to achieve approximate thermal equilibrium. This could be considered as a single heavier component which is Spitzer unstable with respect to the remaining components. This would help to reduce a multi-component system to the two-component case studied in this paper.

Nevertheless, it is not clear quantitatively how the considerations of this research are to be applied to a multi-

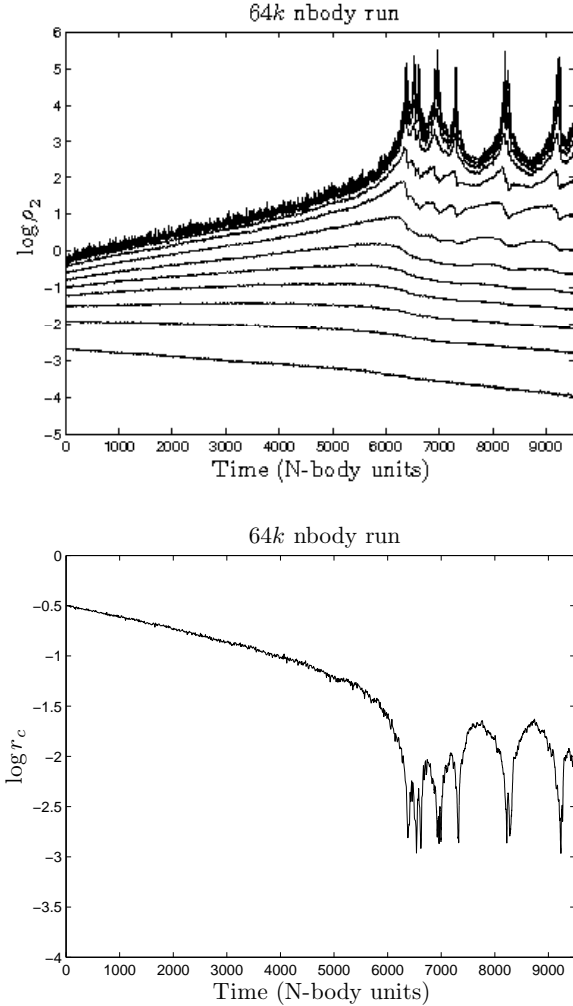


Figure 16. 64k N-body run. Top: $\log \rho_2$ at various Lagrangian shells in the heavier component, bottom: $\log r_c$ vs time

component cluster. Furthermore, we have ignored many things such as primordial binaries, tidal fields and stellar evolution and these are important in the evolution of a real star cluster. Further study is needed in order to understand the phenomenon that is gravothermal oscillation.

ACKNOWLEDGEMENTS

We are indebted to S. Aarseth and K. Nitadori for making publicly available their version of NBODY6 adapted for use with a GPU. We thank the anonymous referee for helping us to clarify the paper. Our hardware was purchased using a Small Project Grant awarded to DCH and Dr M. Ruffert (School of Mathematics) by the University of Edinburgh Development Trust, and we are most grateful for it. PGB is funded by the Science and Technology Facilities Council (STFC).

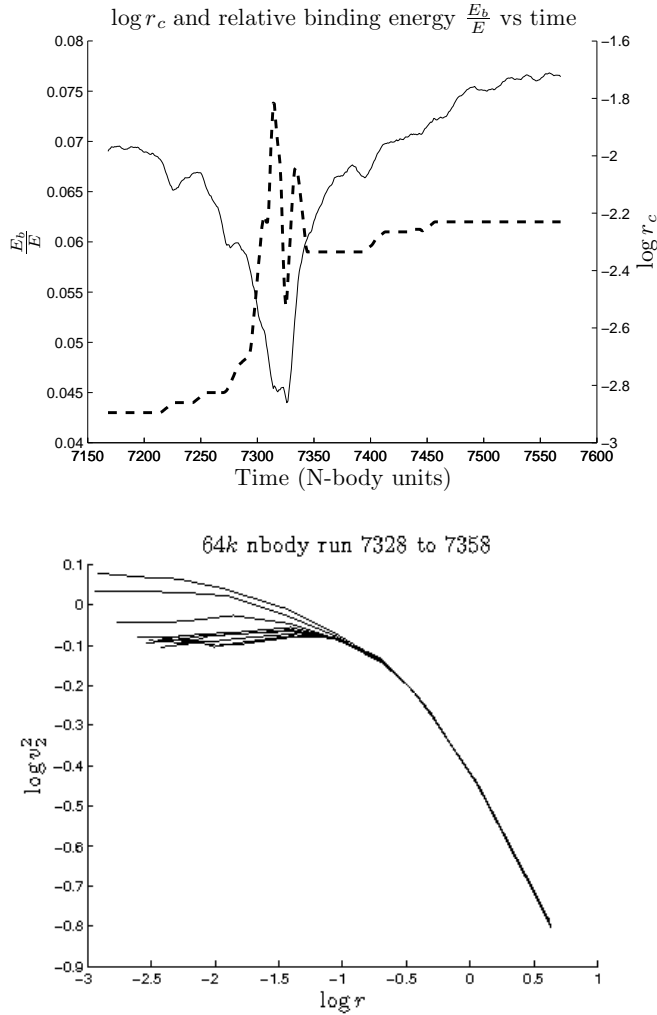


Figure 17. Top: evolution of the relative binding energy $\frac{E_b}{E}$ and $\log r_c$. Bottom: $\log v_2^2$ measured at Lagrangian shells in the heavier component over part of the expansion of the core.

REFERENCES

- Antonov V. A., 1962, Vest. Leningrad Gos. Univ., 7, 135 (English translation in Goodman J., Hut P., eds, IAU Symp. 113, Dynamics of Globular Clusters. Reidel, Dordrecht, p. 525)
- Bettwieser E., Sugimoto D., 1984, MNRAS, 208, 493
- Bettwieser E., Sugimoto D., 1985, MNRAS, 212, 189
- Binney J., Tremaine S., 2008, Galactic Dynamics, Second Edition (Princeton: Princeton University Press)
- Chernoff D.F., Weinberg M.D., 1990, ApJ, 351, 121
- Cohn, H., Hut, P., Wise, M., 1989, ApJ, 342, 814
- Fregeau J.M., Joshi K.J., Portegies Zwart S.F., Rasio F.A., 2002, ApJ, 570, 171
- Giersz M., Heggie D.C., 1996, MNRAS, 279, 1037
- Giersz M., Heggie D.C., 2009, MNRAS, 395, 1173
- Goodman J., 1993, in Structure and Dynamics of Globular Clusters, ASP Conf. Ser. 50, ed. Djorgovski, S.G., Meylan, G., ASP, San Francisco, p. 87
- Goodman J., 1987, ApJ, 313, 576
- Gürkan M.A., Freitag M., Rasio F.A., 2004, ApJ, 604, 632
- Heggie D.C., Aarseth S. J., 1992, MNRAS, 257, 513
- Heggie D.C., Giersz M., 2009, MNRAS, 397, 46
- Heggie D.C., Hut P., 2003, The Gravitational Million Body Problem (Cambridge: Cambridge University Press)
- Heggie D. C., Mathieu, R. D., 1986 in The Use of Supercomputers in Stellar Dynamics, ed. Hut, P., McMillan, S. L. W., Springer-Verlag, Berlin, p.233
- Heggie D.C., Ramamani N., 1989, MNRAS, 237, 757
- Hénon M., 1975, in A. Hayli, ed., Proc. IAU Symp. 69, Dynamics of Stellar Systems. Reidel, Dordrecht, p. 133
- Khalisi E., Amaro-Seoane P., Spurzem R., 2007, MNRAS, 374, 703
- Kim S.S., Lee H.M., 1997, Publ. Korean Astron. Soc., 30(2), 115
- Kim S.S., Lee, H.M., Goodman, J., 1998, ApJ, 495, 786
- Lynden-Bell D., Eggleton P.P., 1980, MNRAS, 191, 483
- Lynden-Bell D., Wood R., 1968, MNRAS, 138, 495
- Makino J., 1996, ApJ, 471, 796
- McMillan S.L.W., Engle E.A., 1996, in IAU Symp. 174, Dynamical Evolution of Star Clusters. Kluwer, Boston, p.379
- Murphy B. W., Cohn H. N., Hut P., 1990, MNRAS, 245, 335

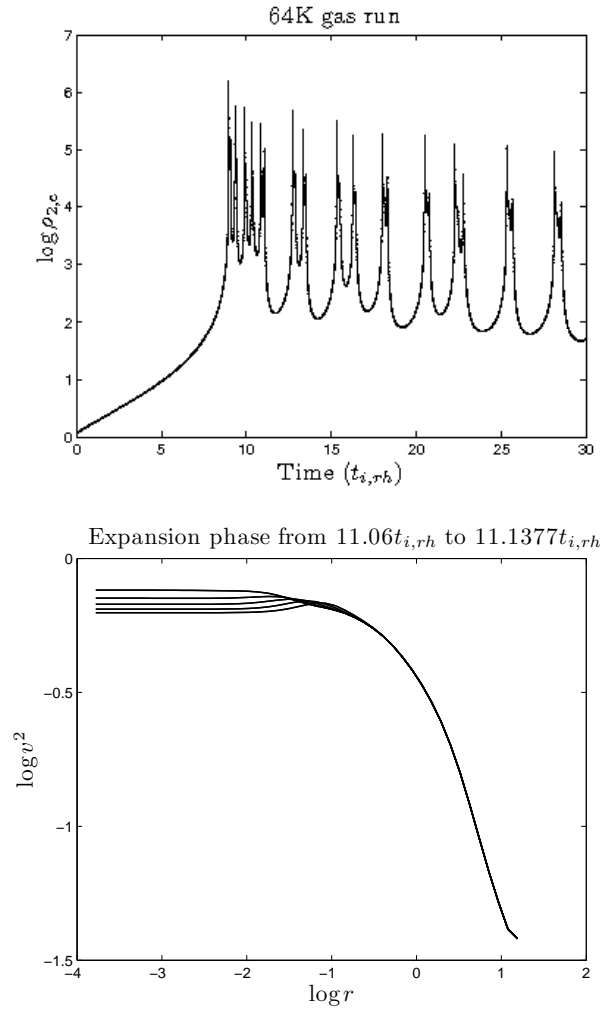


Figure 18. 64k gas model. Top: $\log \rho_{2,c}$ vs time (units $t_{i,rh}$), bottom: $\log v_2^2$ vs $\log r$ at different times during a gravothermal expansion.

- Plummer H.C., 1911, MNRAS, 71, 460
Spitzer L., 1987. Dynamical Evolution of Globular Clusters
(Princeton: Princeton University Press)
Takahashi K., 1995, PASJ, 47, 561
Watters W.A., Joshi K.J., Rasio F.A., 2000, ApJ, 539, 331

This paper has been typeset from a T_EX/ L^AT_EX file prepared
by the author.